Nanoscale

Multilayer electrodeposition of Pt onto 1-2 nm Au nanoparticles using a hydride-termination approach

Journal:	*Nanoscale*
Manuscript ID	NR-ART-04-2020-002929.R1
Article Type:	Paper
Date Submitted by the Author:	11-May-2020
Complete List of Authors:	Crooks, Richard; The University of Texas at Austin Lapp, Aliya S; The University of Texas at Austin

Multilayer electrodeposition of Pt onto 1-2 nm Au nanoparticles using a hydride-termination approach†

Aliya S. Lapp and Richard M. Crooks*

Department of Chemistry and Texas Materials Institute, The University of Texas at Austin, 2506 Speedway, Stop A5300, Austin, TX 78712-1224, U.S.A.

*To whom correspondence should be addressed.

Email: crooks@cm.utexas.edu

Submitted: 13 April, 2020

Revised: 11 May, 2020

Abstract

Here we report on hydride-terminated (HT) electrodeposition of Pt multilayers onto ~1.6 nm Au nanoparticles (NPs). The results build on our earlier findings regarding electrodeposition of a single monolayer of Pt onto Au NPs and reports relating to HT Pt electrodeposition onto bulk Au. In the latter case, it was found that electrodeposition of Pt from a solution containing $PtCl_4^{2-}$ can be limited to a single monolayer of Pt atoms if it is immediately followed by adsorption of a monolayer of H atoms. The H-atom capping layer prevents deposition of Pt multilayers. In the present report we are interested in comparing the structure of NPs after multiple HT Pt electrodeposition cycles to the bulk analog. The results indicate that a greater number of HT Pt cycles are required to electrodeposit both a single Pt monolayer and Pt multilayers onto these Au NPs compared to bulk Au. Additionally, detailed structural analysis shows that there are fundamental differences in the structures of the AuPt materials depending on whether they are prepared on Au NPs or bulk Au. The resulting structures have a profound impact on formic acid oxidation electrocatalysis.

Introduction

In this article, we investigate the use of a hydride-termination (HT) method for the electrodeposition of multiple Pt layers onto small (~1 to 2 nm) Au nanoparticles (NPs). Compared to HT growth on bulk two-dimensional Au surfaces,[1-4] we find that a greater number of electrodeposition steps is required to achieve a single, complete Pt layer, and subsequent Pt multilayers, on Au NPs. Moreover, we find that incremental changes in Pt coverage on Au NPs significantly impact electrocatalytic activity for formic acid oxidation (FAO).

The foregoing results are important for the following reasons. First, core@Pt-shell NPs provide a means for minimizing Pt loading in electrocatalytic devices.[5-7] Therefore, it is important to assess the viability of methods that can be used for depositing thin Pt shells on NPs. Second, HT Pt electrodeposition[1] represents a promising alternative to other core@Pt shell NP synthesis techniques, such as underpotential deposition (UPD) followed by galvanic exchange (GE).[6,8-16] This is because UPD/GE necessitates multiple steps and can lead to NP contamination by residual UPD metal.[15,17-20] The HT approach bypasses these complications by using adsorbed H (H_{ads}) to control the extent of Pt electrodeposition.[1] Third, our results highlight an important difference in physical properties (e.g., geometry) between bulk-phase materials and small NPs.

Pt monolayer (ML) electrodeposition is complicated by the fact that a direct approach typically leads to three-dimensional Pt growth.[21,22] A common method for circumventing this limitation is to electrodeposit a ML of a metal known to provide two-dimensional growth (e.g., UPD of Cu or Pb), and then galvanically exchange the UPD metal for Pt.[6,8–15] However, the UPD/GE route can suffer from the types of problems noted earlier.

HT Pt electrodeposition, pioneered by Moffat and coworkers,[1] is a rapid method for directly electrodepositing a Pt ML onto a second metal substrate. This method consists of three steps (Scheme 1). After cleaning the surface (Step 1), the electrode potential is pulsed (Step 2) to a value wherein hydrogen evolution on Pt is diffusion limited. This latter condition ensures that newly electrodeposited Pt atoms are quickly capped by adsorbed H_{ads}, which limits Pt growth to a single ML. In Step 3, the electrode potential is pulsed positive to remove the H_{ads} layer. Steps 1 to 3 can be repeated to electrodeposit Pt MLs onto bulk materials in an approximately layer-by-layer fashion.[1,2,4,23,24]

HT Pt electrodeposition has previously been demonstrated on bulk Au,[1,2,4,25] nanoporous Au,[26,27] star-shaped dendritic Au rods (DARs),[23,24] Ni,[3,28] and C-based substrates.[29–32] HT electrodeposition has also proven useful for Ir

electrodeposition onto bulk Pt, Au, and Ni,[33] and for synthesizing PtCoNi alloys.[34] Despite the success of the HT method on these substrates, its application on NPs is much less developed. Recently, however, our group examined HT Pt electrodeposition on ~1.6 nm Au NPs.[35] On the basis on Moffat's findings of near-ML Pt coverage (75 to 85%) on bulk Au,[1,2] we expected to find similar structures for Au NPs. A combination of experimental and theoretical investigations revealed, however, that the resulting AuPt NPs were quasi-random alloys rather than well-defined core@shell structures.[35] Moreover, density functional theory-molecular dynamics (DFT-MD) based simulations suggested that the structural divergence between the Pt MLs electrodeposited on bulk Au vs. Au NPs stemmed from inherently dissimilar structural flexibilities.[35] Specifically, the enhanced structural flexibility of small Au NPs was predicted to lead to alloying via rapid (7.5 ps) Pt absorption into the Au lattice. In contrast, the rigidity of bulk Au was predicted to support a segregated Pt ML.

Despite these interesting findings, several questions about the HT Pt electrodeposition process on Au NPs remained unanswered. For example, how many Pt atoms are able to absorb into the Au NP lattice before a structure having a complete Pt shell is produced? Indeed, is it even possible to use the HT

method to prepare core@complete-shell NP structures using multiple HT pulses? The present study addresses these questions.

The growth of consecutive Pt MLs on bulk Au[2,4] and star-shaped DARs[23,24] via the HT method has been used to study the effect of Pt layer thickness on the electrocatalytic FAO reaction,[2,23] the methanol oxidation reaction (MOR),[2,24] and the oxygen reduction reaction (ORR).[4] A few trends are evident from these reports. First, for bulk Au, a complete Pt ML is obtained after one or two iterations of the potential-pulse sequence shown in Scheme 1.[1-4] Second, the number of Pt layers electrodeposited corresponds closely with the number of HT Pt electrodeposition pulses.[1-3] In contrast, when the geometry is changed to star-shaped DARs, 15 iterations of Scheme 1 are required to obtain a complete Pt ML and 30 iterations are needed for the second ML.[23,24] These results indicate that substrate geometry plays an important role in the HT process. Given the promise of the HT method as a less complicated, more versatile, and more direct alternative to UPD/GE for Pt ML electrodeposition, the nuances of its mechanism at different scales and on different geometries are crucial to its widespread application.

In this report, we extend our earlier study, which involved the structure of AuPt NPs produced using a single electrodeposition pulse on ~1.6 nm Au NPs,[35] to structural

evaluation of AuPt NPs prepared using multiple HT pulses. The results of this study provide the following insights. First, electrochemistry, TEM, and XPS indicate that a nearly complete Pt ML is obtained after 3 to 5 pulses. This level of Pt coverage onto small Au NPs, even after this number of electrodeposition steps, is not a foregone conclusion given the high energy associated with corner and edge sites on the Au NPs and the demonstrated propensity for AuPt NP alloying.[35] Second, the fact that a AuPt-core@Pt-shell structure can be obtained, as opposed to the alloy-like structure produced upon a single HT pulse,[35] unlocks the advantages of the HT Pt electrodeposition method for NPs. Third, the number of HT pulses (3 to 5) needed to electrodeposit each Pt ML differs from bulk Au (1 to 2 pulses) and DARs (15 pulses). These results suggest that size and geometry play an important role in the HT method. Fourth, FAO activity is enhanced (5 to 110x) relative to bulk Pt and is tunable based on the number of Pt pulses applied: 1 and 10 HT pulses yield the highest and lowest activity, respectively.

Experimental Section

Chemicals and materials. A 9.0 wt% solution of generation 6.0, poly(amidoamine) dendrimers (G6-NH_2) in methanol was acquired from Dendritech, Inc. (Midland, MI). The methanol was removed by evaporation, and the dendrimers were re-dissolved in water to

yield a 100 μM aqueous stock solution. $HAuCl_4$ (≥99.9%), $NaBH_4$ (99.9%), formic acid (88 to 91%), H_2SO_4 (95 to 98%), HPLC grade isopropanol (99.9%), and a standardized NaOH solution (0.50 M) were purchased from Sigma-Aldrich. NaCl, K_2PtCl_4 (99.9%), and aqueous 70% $HClO_4$ were obtained from Fisher (New Jersey, USA). All solutions were made using deionized (DI) Milli-Q water (18.2 MΩ-cm; Millipore, Bedford, MA). Vulcan carbon (EC-72R) was from ElectroChem, Inc. (Woburn, MA).

Grids for TEM (catalog numbers CF400-Cu-UL and LC400-Cu-UL) were purchased from Electron Microscopy Sciences (Gibbstown, NJ). All electrodes and a 700E potentiostat were acquired from CH Instruments (Austin, TX). The counter, working, and reference electrodes were a glassy carbon rod, a 3.0 mm glassy carbon electrode (GCE), and Hg/Hg_2SO_4 (MSE), respectively. However, all potentials were converted to the reversible hydrogen electrode (RHE) scale.

Synthesis and characterization of Au_{147} dendrimer-encapsulated nanoparticles (DENs). Au_{147} DENs (2.0 μM) were synthesized using a two-step procedure. First, 0.147 mL of $HAuCl_4$ (20.0 mM) was added dropwise, with vigorous stirring, to a solution containing 0.200 mL of G6-NH_2 dendrimers (100 μM) and 8.65 mL of Milli-Q water. Second, <2 min after the first drop of $HAuCl_4$ was added to the dendrimer solution, 0.30 M NaOH (1.0 mL)

was added to an 11-fold excess of $NaBH_4$ (~1.2 mg). The resulting mixture was immediately transferred to the DENs reaction vial. Reduction of the dendrimer-$AuCl_4^-$ composite led to a rapid color change from light yellow to brown. After ~7 min, the stir speed was reduced, and the DENs vial was loosely capped. Excess BH_4^- in the DENs solution was deactivated in air for ≥12 h and then the DENs were characterized.

Au_{147} DENs were characterized using UV-Vis spectroscopy and transmission electron microscopy (TEM). UV-Vis spectroscopy was performed using a Hewlett-Packard 8453 spectrometer, a 2.0 mm quartz cuvette, and Milli-Q water as a reference. For TEM, 2.0 μL of the 2.0 μM Au_{147} DENs solution was dropcast onto a carbon-film-coated Cu grid (CF400-Cu-UL) and dried in air. Standard TEM was carried out using a JEOL 2010F TEM with 0.19 nm point-to-point resolution and an operating voltage of 200 kV. Aberration corrected scanning TEM (acSTEM) and energy dispersive spectroscopy (EDS) was performed using a JEOL NEOARM TEM using an operating voltage of 80 kV and a point-to-point STEM resolution at 80 kV of 0.11 nm.

Electrochemical synthesis and characterization of AuPt DENs. GCEs were polished successively using 1.0, 0.3, and 0.05 μm alumina (2 min/thickness). Subsequent sonication in Milli-Q water (10 min) was used to remove excess alumina from the electrode surface. VC-based inks for electrochemistry were

prepared using the following components: ~1.0 mg VC, 0.20 mL of isopropanol, and 1.0 mL of 2.0 μM Au_{147} DENs. Prior to addition of the DENs, the VC and isopropanol were sonicated together until a homogeneous slurry was obtained (~10 to 15 min). This step aids in dispersion of the hydrophobic VC before it contacts the aqueous DENs solution. After the DENs were added to the VC slurry, the resulting mixture was sonicated for an additional 10 to 15 min. Once the electrochemical ink was prepared, 6.0 μL was dropcast onto a polished 3.0 mm GCE and dried under gently flowing N_2.

Electrochemical cleaning of the Au_{147} DENs was carried out using cyclic voltammetry (CV; 20 cycles) in N_2-purged 0.10 M $HClO_4$. The electrode potential was scanned from 0.70 V to 1.57 V and then back to 0 V, at a scan rate of 200 mV/s. Subsequently, the Au surface area was characterized using the same parameters, but for just three CV cycles and at a scan rate of 100 mV/s.

After Au surface cleaning and characterization, Pt was electrodeposited using the HT method[1,35] in an N_2-purged, pH 4.0 solution containing 0.50 M NaCl and 3.0 mM K_2PtCl_4. The electrodeposition procedure followed that shown in Scheme 1, except that a shorter time (1.0 s) was used for Step 3. For 1 HT pulse, the electrode potential was held at 0.86 V for 30.0 s (Step 1), -0.34 V for 1.0 s (Step 2), and then 0.86 V for 1.0 s

(Step 3). For multiple HT pulses, Steps 1 to 3 were repeated multiple times.

Following HT Pt electrodeposition, a three-step rinsing procedure was used: ~20 s in 250 mL of Milli-Q water, 5 min in 0.10 M $HClO_4$ with vigorous stirring, and ~5 s in 20 mL of Milli-Q water. As we showed in a previous publication,[33] this rinsing procedure prevents adventitious Pt NP formation on the GCE upon subsequent electrochemical cycling. The AuPt NP surfaces were characterized by CV in N_2-purged 0.10 M $HClO_4$ at a scan rate of 100 mV/s. The scan parameters were identical to those used for Au_{147} surface characterization, except that a total of nine cycles were used. After surface characterization, the GCE was rinsed in Milli-Q water and then swiped over the surface of a lacey carbon-coated Cu TEM grid (LC400-Cu-UL) for imaging by TEM.

X-ray photoelectron spectroscopy (XPS). A Kratos Axis Ultra DLD spectrometer (Chestnut Ridge, NY) equipped with an Al K_α source was used for XPS measurements. XPS samples were prepared on TEM grids; after electrochemical characterization and rinsing, the surfaces of the GCEs containing the AuPt DENs were swiped onto lacey carbon-coated Cu TEM grids. Care was taken to fully coat the TEM grid to ensure an adequate XPS signal-to-noise ratio. XPS spectra utilized a band pass energy of 20 eV and a step size of 0.10 eV. Peak positions were calibrated

relative to C 1s (284.5 eV).[11,36,37] A Gaussian/Lorentzian model (GL90) was used to fit the Au 4f peaks, whereas the Pt 4f peaks were fit using an asymmetric Lorentzian model: LA (1.2,85,70).

Formic acid oxidation (FAO). Prior to FAO, a control CV was recorded in N_2-purged, 0.50 M H_2SO_4. Specifically, the electrode was immersed under potential control at 0.01 V. The potential was then cycled two times from 0.01 to 1.26 V and then back to 0.01 V at a scan rate of 10.0 mV/s. After the control CV was recorded, the GCE was removed from the cell and rinsed. Formic acid (0.50 M) was then added to the cell and mixed using N_2 agitation. The same steps as for the control CV were then repeated except, to be consistent with the original report of HT Pt electrodeposition on macro surfaces, 20 cycles were recorded.[2]

Results and Discussion

Electrochemical synthesis and characterization of AuPt DENs.

Au_{147} DENs were synthesized as described in the Experimental Section. Briefly, 147 equiv. of $HAuCl_4$ were added dropwise to an aqueous G6-NH_2 solution with rapid stirring, and then the resulting mixture was reduced with an 11-fold excess of $NaBH_4$. Our previous studies have shown that this synthesis yields ~1 to 2 nm Au NPs that are sterically trapped within the dendrimer and that experience minimal chemical interactions with the dendrimer.[7,12,35,38-40] The Au_{147} DENs synthesized in the present

report have a size distribution of 1.6±0.3 nm (Figure 1a), which is consistent with the theoretically predicted size for a perfect Au_{147} cuboctahedron (1.6 nm).[12,13]

Figure 2a presents a series of CVs obtained as a function of the number of HT pulse sequences (Scheme 1) applied to the GCE-immobilized Au_{147} DENs. The purple trace was obtained prior to Pt electrodeposition. The only notable features are an anodic current positive of ~1.3 V, arising from surface oxidation of the Au_{147} DENs, and the corresponding AuO_x reduction peak (Peak P1) at ~1.1 V. Integration of the area under this latter peak (expanded view in Figure 2b) and conversion of charge to the Au electrochemically active surface area (ECSA), using the generally accepted factor of 390 μC/cm^2,[13,41] yields an average of 0.26±0.03 cm^2 (based on 12 independent experiments).

HT Pt electrodeposition onto the Au_{147} DEN cores was carried out as described in the Experimental Section using the method outlined in Scheme 1. The black trace in Figure 2a was obtained following 1 HT Pt electrodeposition pulse. Compared to the purple CV, Peak P1 decreases and two new peaks emerge: PtO_x reduction (Peak P2) and Pt-H adsorption/desorption (Pt-hydride; Peaks labeled P3). This general trend continues after 3, 5, and 10 HT pulses. For example, Peak P2 increases in magnitude and its potential shifts slightly positive. This positive shift as a function of pulse number is consistent with previous results

obtained for increasing coverages of Pt on Au NPs.[42,43] Additionally, the P3 peaks also grow as a function of the number of HT pulses.

With regard to the Au-related peaks, it is apparent that the area under Peak P1 is still significant after 1 HT pulse. This finding is consistent with our earlier report that focused on just a single HT pulse, and it clearly indicates that the NP surface consists of both Au and Pt atoms.[35] After 3 and 5 HT pulses, however, the area under Peak P1 becomes very small (Figure 2b), suggesting nearly complete Pt coverage of the original Au core. To summarize the qualitative trends in Figures 2a and 2b, the Au NP surface is nearly completely covered by Pt after 3 to 5 HT pulses, and more pulses simply expand the Pt shell. We can learn more about the HT process, however, by quantitatively examining Figures 2a and 2b. For this purpose, we introduce several parameters related to Pt coverage: θ_{Pt}, the Pt:Au_i ECSA ratios, $N_{Au,surf}$, and $\%Pt_{surf}$, all of which are defined in Table 1.

Three quantitative trends confirm the conclusions reported in the previous paragraph. First, the Pt coverage (θ_{Pt}, Table 1) approaches unity after 3 (θ_{Pt}=0.83±0.02) to 5 (θ_{Pt}=0.91±0.01) HT pulses (Figure 2c), confirming that the original Au NP surface is nearly completely covered by Pt. Second, the rate of change in θ_{Pt} (Figure S1) slows as a function of the number of pulses.

Specifically, $\frac{d\theta_{Pt}}{dp}$ approaches zero after 5 HT pulses. Despite slowing growth in θ_{Pt}, the Pt ECSA (Table S1) continues to increase with the number of pulses. Another way of looking at this is to consider the Pt:Au_i ECSA ratio (Table 1), which increases from 1.8±0.2 to 2.6±0.1 after 5 and 10 HT pulses, respectively. The experimental Pt:Au_i ECSA ratios for 5 and 10 pulses match those theoretically predicted (Table S2) for one (1.8) and two (2.7) complete Pt MLs, respectively, on a cuboctahedral Au_{147} NP core. Taken together, these trends support the assertion that the NP shell consists of Pt multilayers after ≥5 HT pulses.

The third point is that the center of Peak P2 in Figure 2a shifts positive by 79 mV as the number of Pt electrodeposition pulses increases from 1 to 10. As shown in Figure 2d, about half of this total shift occurs between pulses 1 and 3. The fact that smaller shifts in the position of Peak P2 occur between 3 and 5 pulses and 5 and 10 pulses suggests that the largest change in Pt electronic properties occurs between 1 and 3 HT pulses. This result is consistent with a transition from sub-ML Pt coverage, where the interplay of ligand, ensemble, and strain effects control the potential at which Pt oxidation occurs,[2,4] to nearly complete ML coverage (after 3 to 5 pulses) where strain effects dominate (and diminish as the number of MLs increase).[4,44]

Although multiple HT pulses are required to fully cover Au_{147} NPs with Pt, the fact that complete Pt coverage is ultimately obtained (after ~5 pulses) is significant for two reasons. First, Au_{147} NPs have a much greater proportion of high energy sites than bulk Au (i.e., 65% corner plus edge atoms).[13,19,45] The results in Table 1 show that after 3 HT pulses there are 16 naked surface Au atoms ($N_{Au,surf}$ = 16). This value is much smaller than the total number of corner and edge sites (60) on Au_{147} NPs, and therefore we conclude that the majority of the high-energy sites are covered with Pt for ≥3 HT pulses. Furthermore, $N_{Au,surf}$ after 3 HT pulses is close to the number of corner sites (12) present on the original Au_{147} NPs. It is possible that these corner sites are not receptive to Pt deposition, and this could account for the slow increase in θ_{Pt} between 3 to 10 HT pulses.

Second, the Pt coverage obtained after 3 to 5 HT pulses (θ_{Pt} = 0.83±0.02 to 0.91±0.01, respectively) is greater than that previously observed using either Pb UPD/Pt GE (~0.50 to 0.57)[12,13,46] or Cu UPD/Pt GE (~0.70 to 0.80)[11,12] to prepare AuPt DENs from Au_{147} DEN cores. This result suggests that the HT method is a viable alternative to UPD/Pt GE for Pt ML electrodeposition on small Au NPs as long as a sufficient number of pulses are used. Additionally, and as alluded to in the introduction, the HT method avoids key complications associated

with UPD/Pt GE, such as residual UPD metal left on the Au surface following GE,[15,17–20] low Pt coverages,[12,47,48] and the need for multiple deposition solutions.[49] Given that just a few residual heteroatoms can alter the catalytic properties of NPs,[19] the HT method provides a cleaner route for synthesizing core@Pt shell electrocatalytic NPs.

Transmission electron microscopy (TEM). TEM micrographs of AuPt DENs synthesized using 1 to 10 HT pulses, and the corresponding size-distribution histograms, are shown in Figure 1. For comparison, theoretical predictions of NP size as a function of the number of Pt MLs electrodeposited are provided in Table S2.

As discussed in the previous section, Figure 1a indicates that the average size distribution of the Au_{147} DENs prior to HT Pt electrodeposition (0 pulses) is 1.6±0.3 nm. Figures 1b and 1c demonstrate that both 1 and 3 HT pulses yield size distributions of 2.6±0.5 nm. Although this size distribution is larger than predicted for a perfect cuboctahedral 309 atom Au@Pt NP (2.3 nm), it is, within error, the same as we have reported for electrodeposition of a single Pt layer on Au_{140} (2.5±0.4 nm)[14] and Au_{147}(2.4±0.4 nm)[12] DENs using UPD/Pt GE. This value is also similar to the one we have previously reported for a single HT pulse on Au_{147} DENs (2.8±0.6 nm).[35] The fact that 1 and 3 HT pulses yield equivalent AuPt NP size distributions is consistent

with the electrochemical results, which showed that at least 3 HT pulses are required to electrodeposit a nearly complete Pt ML.

The size distribution for the AuPt DENs synthesized using 5 HT pulses (Figure 1d) is 3.0±0.5 nm. This size agrees well with the theoretically predicted size for the deposition of 2 ML of Pt on Au_{147} (2.8 nm). The size distribution for 10 HT pulses (Figure 1e) is 3.3±0.6 nm, which is in close agreement with the size theoretically predicted for the deposition of 3 ML of Pt on Au_{147} (3.4 nm). These TEM results are, within 1 ML, the same as that determined electrochemically. As discussed in the next section, the TEM results also closely match XPS data.

X-ray photoelectron spectroscopy (XPS). The NPs used in this study are sufficiently small that XPS provides elemental composition of the entire NP rather than just the surface.[50,51] In contrast, the foregoing electrochemical analysis provides information about just the surface composition. By correlating the XPS and electrochemical results, therefore, it is possible to draw conclusions about NP structure.

XPS spectra for the AuPt DENs synthesized using 1 to 10 HT pulses are shown in Figure 3a. Data for the naked Au_{147} DENs (0 pulses) are also shown. The Au and Pt atomic percentages for each NP composition (Figure 3b) were obtained by integrating the Au 4f and Pt 4f peaks. The number of Pt MLs electrodeposited on

Au_{147} after each HT pulse (Figure S2) was estimated by comparing the experimental compositions to theoretically computed values that assume all Pt is present in the outermost layers of the NPs (i.e., does not alloy into the core; Table S2 and Figure S3).

For 1 HT pulse, comparison of Figures 3b and S3 shows that the percentage of Pt determined by XPS, 39 atomic%, is insufficient to account for electrodeposition of one complete ML of Pt (52 atomic%, Table S2) onto an Au_{147} core. The mismatch in the number of MLs (Figure S2) calculated using the XPS (0.78 ML) and electrochemistry (θ_{Pt}=0.57) data suggests that a fraction of the Pt atoms is alloyed within the NP core. This result is consistent with our past analysis for a single HT pulse on Au_{147}.[35]

For 3 HT pulses, comparison of Figures 3b and S3 shows that the amount of Pt electrodeposited (61 atomic%) is 9% greater than predicted for a single complete Pt ML (52%; Table S2). However, given that the electrochemical results (Table 1) indicate that only ~88% of the surface atoms are Pt after 3 HT pulses, a fraction of the Pt atoms (~45) either alloy into the core or are present as the beginning (~0.2 ML) of a second Pt shell.

After 5 HT pulses, the Pt composition determined by XPS (71 atomic%) is close to that expected for deposition of 2 ML of Pt on Au_{147} (74% atomic Pt, Table S2 and Figure S3). These results

are also in accord with the TEM data discussed earlier, which indicated an average NP size of 3.0 nm. This value is close to that expected for the deposition of 2 ML of Pt (2.8 nm).

For 10 HT pulses, the Pt composition (84 atomic%) exactly matches the expectation for Au_{147} having a Pt shell that is 3 ML thick (Table S2 and Figure S3). TEM data also support this structure: the average NP size (3.3 nm) is very close to that predicted for 3 ML of Pt on Au_{147} (3.4 nm).

The number of HT pulses (3 to 5) required to electrodeposit a single ML of Pt (θ_{Pt} approaches 1.0, $\frac{d\theta_{Pt}}{dp}$~0, and atomic% Pt~52%) on the Au_{147} NP surface differs from both bulk Au (1 to 2 pulses)[1-4] and star-shaped DARs (15).[23,24] Similarly, the number of HT pulses required to electrodeposit a second Pt ML (5 to 10 pulses) also differs from bulk Au (2 to 3 pulses)[1-3] and star-shaped DARs (30).[23,24] Accordingly, geometry appears to be an important consideration for HT Pt electrodeposition. This may be because small Au NPs have an increased tendency to alloy with deposited Pt relative to bulk Au.[12,35] Indeed, we have previously shown that a single HT pulse on Au_{147} NPs results in an AuPt alloy structure.[35] In that case, theoretical calculations predicted that alloying would occur via absorption of Pt into the Au_{147} NP lattice, which is more flexible than that of bulk Au.[35]

Energy dispersive spectroscopy (EDS). Single-particle EDS for the AuPt DENs prepared using 10 HT pulses is shown in Figure 4. A core@shell structure is observed (Figure 4a), with Pt (Figure 4b) concentrated towards the edges and Au (Figure 4c) at the center of the NP. The line profiles extracted from the combined map (Figure 4d) and recorded directly (to increase the line profile counts; Figure S4) confirm this assessment.

EDS maps for 1, 3, and 5 pulses are shown in Figures S5 to S8. These maps are less conclusive than those for 10 HT pulses due to smaller NP sizes and corresponding lower EDS counts. Additionally, the smallest AuPt DENs (prepared using 1 to 3 HT pulses) were easily damaged by the electron beam. As a result, it was challenging to find a sufficient number of NPs that were stable under the beam to collect the statistics necessary for definitive conclusions. With these caveats in mind, EDS maps for 1 HT pulse (Figure S5a to S5c) suggest an alloy structure, as indicated by overlapping Pt and Au signals. The line scan (Figure S5d) extracted from the map in Figure S5a supports this claim. However, low counts in Figure S5d prevent definitive conclusions. Direct line scans (as opposed to extraction from the map) over half of the NP provide higher counts and resolution, due to lower collection times and the greater number of points collected per nm. An atomic resolution line scan of the AuPt DENs synthesized via 1 HT pulse (Figure S6) suggests

that alloying is localized in the NP shell. In other words, 1 HT pulse appears to lead to a surface alloy, which is consistent with our previous report for 1 HT pulse on Au_{147} DENs.[35]

An EDS map for the AuPt DENs synthesized using 3 HT pulses is shown in Figure S7. For the combined Au plus Pt map, it appears that Pt is localized in the NP shell (Figure S7a). Two cautionary points should be mentioned, however. First, if a Pt shell is present, it is not complete, as indicated by the presence of a few regions in the outermost layer of the NP that are dominated by Au atoms (green pixels). This result supports the electrochemical data discussed earlier, which showed that ~17% of the NP surface is Au. Second, although the combined Au plus Pt map looks core@shell-like, the individual Pt and Au maps (Figures S7b and S7c) indicate that this is an oversimplification. For example, Figure S7b reveals that Pt is present throughout the NP, while Figure S7c suggests more preference for Au in the NP core than in the shell. Taken together, the EDS data suggest that the most appropriate structure is that of an alloy core@Pt shell.

To gain further clarity about the 3 HT-pulse structure, atomic resolution line scans were obtained (Figure S7d). It should be noted that the oscillations in the Pt signals align roughly with the spacing between the atomic columns. As shown in Figure S7d, the first ~0.3 nm (first atomic column) of the line

scan is predominantly Pt. This suggests the presence of a Pt shell in the outermost layer of the NP, given that an ~0.3 nm increase per side (~0.6 nm total) is expected (Table S2) upon the deposition of a single Pt ML on an ideal cuboctahedral Au_{147} NP. Beyond this point (>0.3 nm), the Pt EDS counts remain approximately constant, while the Au EDS counts increase. Approximately equal Pt and Au EDS counts in the center of the NP suggest that the NP core is alloyed. We reiterate, however, that our conclusions are limited by the small number of line scans that were collected (N=6 line scans for 3 HT pulses).

EDS maps for 5 HT pulses are shown in Figure S8a to S8c, and here a clearer core@shell-like structure is observed. An atomic resolution line scan (Figure S8d) confirms the presence of a Pt shell for 5 pulses. Specifically, Pt is present within the first two atomic columns, suggesting 2 ML of Pt in the shell. Beyond that point, Au and Pt are mixed. This result agrees with the number of Pt MLs predicted by XPS for 5 HT pulses. We do note, however, that some heterogeneity in shell thickness is observed (e.g., Figure S8e). For the eight line scans obtained for the 5 HT-pulse NPs, the average Pt shell thickness is 0.6±0.2 nm on either side of the Au NP core (adding ~1.2 nm total diameter to the NP). Using the expected size changes predicted upon Pt deposition on Au_{147} NPs as a guide

(Table S2), the Pt shell thickness estimated by EDS corresponds to ~1 to 3 ML of Pt.

To summarize, although a single HT pulse on Au_{147} DENs generates an alloy, as supported here and in our previous report,[35] EDS shows that the structure transforms to core@shell after 5 to 10 HT pulses. The fact that alloying is observed for 1 to 3 HT pulses, but that 10 pulses results in an Au@Pt core@shell structure is not completely surprising. It is well known that bulk Au and Pt are immiscible over a broad compositional range.[52] Although AuPt alloying can be facilitated by NP size effects,[35,53] previous theoretical simulations have shown that 2.7 to 4.3 nm AuPt NPs transition to a core@shell structure when atomic% Pt surpasses ~60%.[53] This prediction is consistent with the transition to a core@shell structure in the present report (5 to 10 HT pulses; Figure 3b).

Formic acid oxidation (FAO) electrocatalysis. The preceding sections showed that multilayer HT Pt electrodeposition onto Au_{147} DENs leads to different structures than on bulk Au[1–4] or star-shaped DARs.[23,24] The present section serves to compare the implications of these differences for FAO catalysis and to further validate the structural assignments made earlier.

The FAO experiments were carried out using Au_{147} DENs subjected to 1, 3, 5, and 10 HT pulses. Specifically, CVs were obtained by cycling each AuPt DEN-modified electrode 20 times

between 0.01 and 1.26 V in N_2-purged 0.50 M H_2SO_4 containing 0.50 M formic acid. To be consistent with previous FAO studies obtained using HT-electrodeposited Pt MLs on bulk Au[2] and DARs,[23] we focus only on the forward-going scan of the 20th FAO CVs for each pulse sequence.

The two peaks in each forward-going scan of the FAO CVs for the AuPt DENs prepared using 1 to 10 HT pulses are shown in Figure 5a. These peaks correspond to the two major FAO pathways: (1) direct oxidation to CO_2 (eq 1), and (2) indirect oxidation via a CO intermediate (eq 2).[54–57]

$$HCOOH^* \rightarrow CO_2 + 2H^+ + 2e^- \quad \text{(eq 1)}$$

$$HCOOH^* \rightarrow CO^* + H_2O^* \rightarrow CO_2 + 2H^+ + 2e^- \quad \text{(eq 2)}$$

The peak potentials for the direct pathway for the AuPt DENs (E_d, Table 2; larger peak in the range ~0.42 to 0.52 V in Figure 5a) are negative of E_d for bulk Pt (~0.57 to 0.59 V)[2,46] and for Pt-only DENs (~0.58 V)[46] regardless of the number of HT pulses. As shown in Figure 5b, however, E_d for the AuPt DENs more closely approaches that of monometallic Pt as the number of pulses increases. This suggests that the surface of the NPs becomes increasingly Pt-like with each additional HT pulse.

Figure 5c shows the trend in the peak potentials for the indirect pathway (E_{ind}) as a function of pulse number. For the

AuPt DENs prepared using 1 to 3 HT pulses, E_{ind} (Table 2; 0.905 to 0.926 V) is positive of bulk Pt (~0.85 V).[46] However, after 3 HT pulses, E_{ind} (0.905±0.008 V) is close to that for Pt DENs (~0.91 V).[46] This result supports the surface characterization discussed earlier (Table 1), which showed nearly complete Pt coverage (θ_{Pt}=0.83±0.02) after 3 HT pulses. Comparison of Figures 5b and 5c shows that the position of E_{ind} is less sensitive to HT pulse number than E_d. Furthermore, the shifts in E_{ind} for the AuPt DENs relative to the corresponding values for bulk Pt[2,46] and Pt DENs[46] are less pronounced than for E_d. These results are consistent with a previous report showing similar trends for AuPt DENs prepared by Pb UPD/Pt GE.[46]

The trends in FAO peak potentials as a function of HT pulse number (Figures 5b and 5c) are similar to the corresponding trends for HT-electrodeposited Pt MLs on bulk Au.[2] However, in the latter case, the bulk Pt value for E_d was reached after 5 HT pulses.[2] For the AuPt DENs reported here, even after 10 HT pulses (2 to 3 ML of Pt), E_d (0.515±0.009 V) remains negative of that for bulk Pt[2,46] and Pt DENs.[46] This difference highlights the structural distinctions between HT-electrodeposited Pt MLs on small Au NPs and bulk Au.

In addition to shifts in FAO peak potentials, FAO activity changes as a function of HT pulse number. A recent mechanistic study showed that indirect FAO requires ensembles containing ≥2

adjacent Pt atoms to separately bind CO and OH dissociated from the C-OH bond of carboxylate.[55] Direct FAO, on the other hand, requires just a single Pt atom.[57–59] Thus, in cases with sufficiently large Pt ensembles, the ratio of the current densities for the direct (j_d) and indirect (j_{ind}) peaks (e.g., j_d/j_{ind}) reflects the relative proportions of ensembles containing multiple Pt atoms and single Pt atoms. The fraction of sites containing single Pt atoms is governed by both Pt coverage and AuPt atom arrangement (e.g., alloy vs. core@shell).

The AuPt DENs prepared with a single HT pulse exhibit the highest activity (highest j_d) and the greatest promotion of the direct pathway (highest j_d/j_{ind}) (Figure 5d). The high j_d/j_{ind} ratio indicates extensive mixing of Au and Pt surface atoms; this fact is consistent with the alloy structure previously determined for a single HT pulse on Au_{147} DENs.[35] As the HT pulse number increases, both j_d and j_d/j_{ind} decrease in the direction of the corresponding value for bulk Pt.[2] Figure 5d shows that the rate of change in j_d/j_{ind} as a function of pulse number approaches zero after ~5 HT pulses. Accordingly, the catalytic data supports the conclusion drawn from the ECSA ratios and XPS (Figure S2), that almost 1 Pt ML (θ_{Pt}=0.83 to 0.91 and $\frac{d\theta_{Pt}}{dp}$ ~0) is achieved after 3 to 5 HT pulses. These results can be understood using the framework of the ensemble effects expected for each pulse number. Table 1 shows that the initial number of surface

Au atoms is small for 3 HT pulses ($N_{Au,surf}$ = 16), and becomes negligible thereafter ($N_{Au,surf}$ = 3 to 8 for 5 to 10 HT pulses). Therefore, due to the scarcity of surface Au atoms, the influence of ensemble effects on FAO is expected to be minimal after 3 to 5 pulses.[55] In other words, the trends in j_d/j_{ind} as a function of HT pulse number (Figure 5d) are in accord with the trends in $N_{Au,surf}$ (Table 1). Furthermore, the fact that the indirect FAO pathway becomes dominant (j_d/j_{ind} <1) after 5 HT pulses is consistent with the structural motifs observed via EDS.

To summarize, the individual j_d/j_{ind} ratios for AuPt DENs prepared using 1 to 10 HT pulses (Table 2) are ~5 to 110x higher than for FAO on bulk polycrystalline Pt under similar electrochemical conditions.[2] Likewise, j_d/j_{ind} for the AuPt DENs is ~2-, 5-, and 7-fold greater than for HT Pt electrodeposition onto bulk Au for 1, 3, and 5 HT pulses, respectively.[2] This reflects the fact that there is not as close of a correspondence between the number of HT pulses and the number of Pt MLs on Au_{147} DENs as there is for bulk Au. For example, for the AuPt DENs prepared using 10 HT pulses, j_d/j_{ind} (0.25±0.04) is closest to the corresponding bulk Au results for just 3 HT pulses (j_d/j_{ind} ~0.3).[2]

Further corroboration of the number of Pt MLs determined in the previous sections can be gained by comparing the forward-

going scans of the 20th FAO CVs (Figure 5a) with the forward-going scans of the first FAO CVs (Figure S9a). Comparison of the values of θ_{Pt} before (Table 1) and after (Table S3) recording 20 FAO CVs, shows that θ_{Pt} decreases upon FAO cycling. The magnitudes of the associated changes in θ_{Pt} ($\Delta\theta_{Pt}$) are listed in Table S3. A decrease in θ_{Pt} upon extended FAO cycling has previously been attributed to Pt dissolution and/or structural rearrangement via alloying.[2,42] The $\Delta\theta_{Pt}$ values in Table S3 agree well with those calculated (~0.1 to 0.3 ML for the AuPt DENs) based on previous Pt dissolution studies that employed similar electrochemical conditions.[2,60]

Whether dissolution or alloying, the surface Pt atoms directly above or adjacent to Au atoms are the most vulnerable to loss. Accordingly, a decrease in θ_{Pt} is anticipated for AuPt DENs having ≤1 ML of Pt (3 to 5 HT pulses) but not Pt multilayers (5 to 10 HT pulses). Table S3 shows that the values of $\Delta\theta_{Pt}$ observed for 1 to 20 FAO cycles are consistent with these hypotheses. Specifically, $\Delta\theta_{Pt}$ is significant (0.23 to 0.30) for 1 to 5 HT pulses, but it is negligible for 10 HT pulses (0.03±0.01). These results help confirm the conclusion from the previous sections that 3 to 5 HT pulses are required to completely cover the Au_{147} core with Pt.

The loss in surface Pt observed after 20 FAO cycles enhances ensemble effects for the thinnest Pt layers by enriching the number of surface ensembles that contain both Au and Pt. As mentioned earlier, multiple effects (ensemble, ligand, and strain) are present for <1 ML of Pt on Au.[4,61] For ≥1 ML of Pt, however, strain dominates due to uniform surface ensembles (all Pt) and a progressive lessening of the influence of heteroatoms in atomic sub-layers.[2,4] Thus, comparison of the forward-going scans for the first and 20th FAO CVs aids deconvolution of competing electrocatalytic factors.

Figures 5e and 5f show that j_d/j_{ind} doubles in going from 1 to 20 FAO cycles for the AuPt DENs having the highest values of $\Delta\theta_{Pt}$ (1 to 3 HT pulses, black and blue data points, respectively; Table S3). In contrast, the AuPt DENs with negligible values of $\Delta\theta_{Pt}$ (5 to 10 HT pulses, green and red data points, respectively) show little improvement in j_d/j_{ind}. The correspondence between altered catalytic activity and $\Delta\theta_{Pt}$ confirms the principal role of ensemble effects in catalytic improvement for the FAO using AuPt DENs. Additionally, Figures S9b and S9c reveal that E_d and E_{ind} shift further away from the corresponding values for bulk Pt[2,46] and Pt DENs[46] for 1 to 3 HT pulses (≤1 ML of Pt) after 20 FAO cycles. For 5 (1 to 2 ML of Pt) and 10 HT pulses (2 to 3 ML of Pt), peak positions remain approximately the same between one and 20 FAO cycles.

In summary, significant changes in j_d/j_{ind}, E_d, and E_{ind} between one and 20 FAO cycles are only observed from 1 to 5 HT pulses. These results are consistent with conclusions about the surface and atomic compositions determined from electrochemistry and XPS (Figure S2): ~1 ML of Pt is electrodeposited by 3 to 5 HT pulses and multilayers are electrodeposited for 5 to 10 HT pulses. We reiterate that this scenario is quite different from the results obtained for HT Pt electrodeposition onto bulk Au[1–4] and DARs.[23,24]

Summary and Conclusions

In this report, we have demonstrated several important points relating to the HT Pt electrodeposition process. First, the application of multiple HT Pt pulses to electrodeposit Pt multilayers leads to significantly different results for small (~1 to 2 nm) Au NPs as compared to bulk Au[1–4] and star-shaped DARs.[23,24] Specifically, the number of HT pulses (3 to 5) required to electrodeposit nearly one complete Pt ML is higher than for bulk Au (1 to 2)[1–4] but lower than for DARs (15).[23,24] Similarly, the threshold number of HT pulses (5 to 10) necessary for Pt multilayer electrodeposition onto small Au NPs also diverges from that of bulk Au (2 to 3)[1–4] and DARs (30).[23,24] Thus, we find that HT Pt electrodeposition is highly sensitive to the geometry of the substrate.

Second, our results suggest that the HT method could serve as a viable alternative to UPD/Pt GE for Pt ML electrodeposition on small Au NPs. Importantly, the HT method avoids complications associated with the latter method such as residual UPD metal and the necessity of using multiple deposition solutions.[15,17–20] Furthermore, the HT method is rapid, requiring only ~90 to 150 s (3 to 5 pulses) to electrodeposit ~1 Pt ML onto Au NPs.

Third, we showed that application of multiple HT pulses (1 to 10) on Au NPs can be used to tune their catalytic activity for the FAO. The ratio of the current densities for the direct and indirect FAO processes are ~5- to 110-fold greater than for bulk Pt and also substantially higher than for HT Pt electrodeposition onto other types of Au substrates.[2]

The findings reported here have several possible extensions. First, although our results suggested that the HT method depends on geometry, NP size effects are likely also important. Future studies, such as varying the size and geometry of the Au NP substrate, will be aimed at deconvolving these two factors. Additionally, facet selectivity might prove important for larger NPs and/or more highly faceted substrates. Second, the underlying mechanism for the AuPt structures formed as a function of HT pulse number is unclear at this point. This point will, however, be explored in due course. Third, multilayer shells containing ≤3 MLs of Pt on the Au NPs were studied in

this first report. Examining Pt multilayers having a greater number of MLs could help elucidate the boundary between AuPt NP and bulk Pt behavior. Furthermore, the FAO is more heavily influenced by ensemble effects than strain.[2] Studying a reaction that is more sensitive to the effects of strain (e.g., the ORR)[4] could provide further insight into determining the NP/bulk boundary in these materials. Finally, application of HT Pt multilayer electrodeposition to NPs with different core metals (monometallic and/or bimetallic) could broaden the scope of the results presented here.

Conflicts of Interest

The authors declare no conflict of interest.

Acknowledgements

We gratefully acknowledge financial support provided by the National Science Foundation (Grant: CHE-1855980) and the Robert A. Welch Foundation (Grant: F-0032). We would also like to thank Dr. Hao Li (Technical University of Denmark, Department of Physics) for simulating the theoretical NP diameters listed in Table S2.

Footnote

†Electronic supplementary information (ESI) available: Supplemental figures and tables relating to Pt coverage, electrochemically active surface areas (ECSAs), comparison of theoretically predicted electrochemistry, TEM, and XPS parameters with experiment, additional EDS data, and the effects of extended FAO cycling on Pt coverage and ECSA. See DOI:

References

1. Y. Liu, D. Gokcen, U. Bertocci and T. P. Moffat, Self-Terminating Growth of Platinum Films by Electrochemical Deposition, *Science*, 2012, **338**, 1327–1330.
2. S. H. Ahn, Y. Liu and T. P. Moffat, Ultrathin Platinum Films for Methanol and Formic Acid Oxidation: Activity as a Function of Film Thickness and Coverage, *ACS Catal.*, 2015, **5**, 2124–2136.
3. Y. Liu, C. M. Hangarter, D. Garcia and T. P. Moffat, Self-terminating electrodeposition of ultrathin Pt films on Ni: An active, low-cost electrode for H2 production, *Surf. Sci.*, 2015, **631**, 141–154.
4. Y.-J. Deng, V. Tripkovic, J. Rossmeisl and M. Arenz, Oxygen Reduction Reaction on Pt Overlayers Deposited onto a Gold Film: Ligand, Strain, and Ensemble Effects, *ACS Catal.*, 2016, **6**, 671–676.
5. Y. Zhang, Y.-C. Hsieh, V. Volkov, D. Su, W. An, R. Si, Y. Zhu, P. Liu, J. X. Wang and R. R. Adzic, High Performance Pt Monolayer Catalysts Produced via Core-Catalyzed Coating in Ethanol, *ACS Catal.*, 2014, **4**, 738–742.
6. K. Sasaki, H. Naohara, Y. Cai, Y. M. Choi, P. Liu, M. B. Vukmirovic, J. X. Wang and R. R. Adzic, Core-Protected Platinum Monolayer Shell High-Stability Electrocatalysts for

Fuel-Cell Cathodes, *Angew. Chem. Int. Ed.*, 2010, **49**, 8602–8607.

7. R. M. Anderson, D. F. Yancey, L. Zhang, S. T. Chill, G. Henkelman and R. M. Crooks, A Theoretical and Experimental Approach for Correlating Nanoparticle Structure and Electrocatalytic Activity, *Acc. Chem. Res.*, 2015, **48**, 1351–1357.
8. K. Sasaki, H. Naohara, Y. Choi, Y. Cai, W.-F. Chen, P. Liu and R. R. Adzic, Highly Stable Pt Monolayer on PdAu Nanoparticle Electrocatalysts for the Oxygen Reduction Reaction, *Nat. Commun.*, 2012, **3**, 2124.
9. S. R. Brankovic, J. X. Wang and R. R. Adzic, Metal monolayer deposition by replacement of metal adlayers on electrode surfaces, *Surf. Sci.*, 2001, **474**, L173–L179.
10. J. Zhang, K. Sasaki, E. Sutter and R. R. Adzic, Stabilization of Platinum Oxygen-Reduction Electrocatalysts Using Gold Clusters, *Science*, 2007, **315**, 220–222.
11. D. F. Yancey, E. V. Carino and R. M. Crooks, Electrochemical Synthesis and Electrocatalytic Properties of Au@Pt Dendrimer-Encapsulated Nanoparticles, *J. Am. Chem. Soc.*, 2010, **132**, 10988–10989.
12. A. S. Lapp, Z. Duan, G. Henkelman and R. M. Crooks, Combined Experimental and Theoretical Study of the Structure of AuPt Nanoparticles Prepared by Galvanic Exchange, *Langmuir*, 2019,

35, 16496–16507.

13. D. F. Yancey, L. Zhang, R. M. Crooks and G. Henkelman, Au@Pt dendrimer encapsulated nanoparticles as model electrocatalysts for comparison of experiment and theory, *Chem. Sci.*, 2012, **3**, 1033–1040.
14. L. Luo, L. Zhang, G. Henkelman and R. M. Crooks, Unusual Activity Trend for CO Oxidation on PdxAu140-x@Pt Core@Shell Nanoparticle Electrocatalysts, *J. Phys. Chem. Lett.*, 2015, **6**, 2562–2568.
15. N. Dimitrov, Recent Advances in the Growth of Metals, Alloys, and Multilayers by Surface Limited Redox Replacement (SLRR) Based Approaches, *Electrochim. Acta*, 2016, **209**, 599–622.
16. R. R. Adzic, J. Zhang, K. Sasaki, M. B. Vukmirovic, M. Shao, J. X. Wang, A. U. Nilekar, M. Mavrikakis, J. A. Valerio and F. Uribe, Platinum Monolayer Fuel Cell Electrocatalysts, *Top. Catal.*, 2007, **46**, 249–262.
17. J. Nutariya, M. Fayette, N. Dimitrov and N. Vasiljevic, Growth of Pt by surface limited redox replacement of underpotentially deposited hydrogen, *Electrochim. Acta*, 2013, **112**, 813–823.
18. M. Fayette, Y. Liu, D. Bertrand, J. Nutariya, N. Vasiljevic and N. Dimitrov, From Au to Pt via surface limited redox replacement of Pb UPD in one-cell configuration, *Langmuir*,

2011, **27**, 5650–5658.

19. L. Luo, L. Zhang, Z. Duan, A. S. Lapp, G. Henkelman and R. M. Crooks, Efficient CO Oxidation Using Dendrimer-Encapsulated Pt Nanoparticles Activated with <2% Cu Surface Atoms, *ACS Nano*, 2016, **10**, 8760–8769.
20. Y.-G. Kim, J. Y. Kim, D. Vairavapandian and J. L. Stickney, Platinum Nanofilm Formation by EC-ALE via Redox Replacement of UPD Copper: Studies Using in-Situ Scanning Tunneling Microscopy, *J. Phys. Chem. B*, 2006, **110**, 17998–18006.
21. S. Xie, S.-I. Choi, N. Lu, L. T. Roling, J. A. Herron, L. Zhang, J. Park, J. Wang, M. J. Kim, Z. Xie, M. Mavrikakis and Y. Xia, Atomic Layer-by-Layer Deposition of Pt on Pd Nanocubes for Catalysts with Enhanced Activity and Durability toward Oxygen Reduction, *Nano Lett.*, 2014, **14**, 3570–3576.
22. S. Brimaud and R. J. Behm, Electrodeposition of a Pt Monolayer Film: Using Kinetic Limitations for Atomic Layer Epitaxy, *J. Am. Chem. Soc.*, 2013, **135**, 11716–11719.
23. H. Jeong and J. Kim, Insights into the Electrooxidation Mechanism of Formic Acid on Pt Layers on Au Examined by Electrochemical SERS, *J. Phys. Chem. C*, 2016, **120**, 24271–24278.
24. H. Jeong and J. Kim, Methanol dehydrogenation reaction at Au@Pt catalysts: Insight into the methanol electrooxidation,

Electrochim. Acta, 2018, **283**, 11–17.

25. J. H. K. Pfisterer, Y. Liang, O. Schneider and A. S. Bandarenka, Direct instrumental identification of catalytically active surface sites, *Nature*, 2017, **549**, 74–77.
26. E. Lee, M. Sung, Y. Wang and J. Kim, Atomic Layer Electrodeposition of Pt on Nanoporous Au and its Application in pH Sensing, *Electroanalysis*, 2018, **30**, 2028–2034.
27. Y. Wang and J. Kim, Oxygen Evolution Reaction on Nanoporous Gold Modified with Ir and Pt: Synergistic Electrocatalysis between Structure and Composition, *Electroanalysis*, 2019, **31**, 1026–1033.
28. M. Li, Q. Ma, W. Zi, X. Liu, X. Zhu and S. Liu, Pt monolayer coating on complex network substrate with high catalytic activity for the hydrogen evolution reaction, *Sci. Adv.*, 2015, **1**, e1400268.
29. L. Pang, Y. Zhang and S. Liu, Monolayer-by-monolayer growth of platinum films on complex carbon fiber paper structure, *Appl. Surf. Sci.*, 2017, **407**, 386–390.
30. G. Ercolano, F. Farina, S. Cavaliere, D. J. Jones and J. Roziere, Towards ultrathin Pt films on nanofibres by surface-limited electrodeposition for electrocatalytic applications, *J. Mater. Chem. A*, 2017, **5**, 3974–3980.
31. H. Kim, S. Choe, H. Park, J. H. Jang, S. H. Ahn and S.-K.

Kim, An extremely low Pt loading cathode for a highly efficient proton exchange membrane water electrolyzer, *Nanoscale*, 2017, **9**, 19045–19049.

32. M. A. Alpuche-Aviles, F. Farina, G. Ercolano, P. Subedi, S. Cavaliere, D. J. Jones and J. Roziere, Electrodeposition of Two-Dimensional Pt Nanostructures on Highly Oriented Pyrolytic Graphite (HOPG): The Effect of Evolved Hydrogen and Chloride Ions, *Nanomaterials*, 2018, **8**, 668.
33. S. H. Ahn, H. Tan, M. Haensch, Y. Liu, L. A. Bendersky and T. P. Moffat, Self-terminated electrodeposition of iridium electrocatalysts, *Energy Environ. Sci.*, 2015, **8**, 3557–3562.
34. C. M. Hangarter, Y. Liu, D. Pagonis, U. Bertocci and T. P. Moffat, Electrodeposition of Ternary Pt100-x-yCoxNiy Alloys, *J. Electrochem. Soc.*, 2014, **161**, D31–D43.
35. A. S. Lapp, Z. Duan, N. Marcella, L. Luo, A. Genc, J. Ringnalda, A. I. Frenkel, G. Henkelman and R. M. Crooks, Experimental and Theoretical Structural Investigation of AuPt Nanoparticles Synthesized Using a Direct Electrochemical Method, *J. Am. Chem. Soc.*, 2018, **140**, 6249–6259.
36. R. M. Anderson, D. F. Yancey, J. A. Loussaert and R. M. Crooks, Multistep Galvanic Exchange Synthesis Yielding Fully Reduced Pt Dendrimer-Encapsulated Nanoparticles, *Langmuir*, 2014, **30**, 15009–15015.

37. N. Ostojic, J. H. Thorpe and R. M. Crooks, Electron Transfer Facilitated by Dendrimer-Encapsulated Pt Nanoparticles Across Ultrathin, Insulating Oxide Films, *J. Am. Chem. Soc.*, 2016, **138**, 6829–6837.

38. R. W. J. Scott, O. M. Wilson and R. M. Crooks, Synthesis, Characterization, and Applications of Dendrimer-Encapsulated Nanoparticles, *J. Phys. Chem. B*, 2005, **109**, 692–704.

39. V. S. Myers, M. G. Weir, E. V. Carino, D. F. Yancey, S. Pande and R. M. Crooks, Dendrimer-encapsulated nanoparticles: New synthetic and characterization methods and catalytic applications, *Chem. Sci.*, 2011, **2**, 1632–1646.

40. J. C. Garcia-Martinez and R. M. Crooks, Extraction of Au Nanoparticles Having Narrow Size Distributions from Within Dendrimer Templates, *J. Am. Chem. Soc.*, 2004, **126**, 16170–16178.

41. S. Trasatti and O. A. Petrii, Real surface area measurements in electrochemistry, *Pure Appl. Chem.*, 1991, **63**, 711–734.

42. W. Hong and C. W. Li, Microstructural Evolution of Au@Pt Core-Shell Nanoparticles under Electrochemical Polarization, *ACS Appl. Mater. Interfaces*, 2019, **11**, 30977–30986.

43. M. N. Krstajic Pajic, S. I. Stevanovic, V. V. Radmilovic, A. Gavrilovic-Wohlmuther, P. Zabinski, N. R. Elezovic, V. R. Radmilovic, S. L. Gojkovic and V. M. Jovanovic, Dispersion effect in formic acid oxidation on PtAu/C nanocatalyst

prepared by water-in-oil microemulsion method, *Appl. Catal. B*, 2019, **243**, 585–593.

44. Y. Yu, K. H. Lim, J. Y. Wang and X. Wang, CO Adsorption Behavior on Decorated Pt@Au Nanoelectrocatalysts: A Combined Experimental and DFT Theoretical Calculation Study, *J. Phys. Chem. C*, 2012, **116**, 3851–3856.
45. E. V. Carino and R. M. Crooks, Characterization of Pt@Cu Core@Shell Dendrimer-Encapsulated Nanoparticles Synthesized by Cu Underpotential Deposition, *Langmuir*, 2011, **27**, 4227–4235.
46. R. Iyyamperumal, L. Zhang, G. Henkelman and R. M. Crooks, Efficient Electrocatalytic Oxidation of Formic Acid Using Au@Pt Dendrimer-Encapsulated Nanoparticles, *J. Am. Chem. Soc.*, 2013, **135**, 5521–5524.
47. Y. Yu, Y. Hu, X. Liu, W. Deng and X. Wang, The study of Pt@Au electrocatalyst based on Cu underpotential deposition and Pt redox replacement, *Electrochim. Acta*, 2009, **54**, 3092–3097.
48. S. W. T. Price, J. D. Speed, P. Kannan and A. E. Russell, Exploring the First Steps in Core-Shell Electrocatalyst Preparation: In Situ Characterization of the Underpotential Deposition of Cu on Supported Au Nanoparticles, *J. Am. Chem. Soc.*, 2011, **133**, 19448–19458.
49. M. Fayette, Y. Liu, D. Bertrand, J. Nutariya, N. Vasiljevic

and N. Dimitrov, From Au to Pt via Surface Limited Redox Replacement of Pb UPD in One-Cell Configuration, *Langmuir*, 2011, **27**, 5650–5658.

50. A. Jablonski and C. J. Powell, Information depth and the mean escape depth in Auger electron spectroscopy, and x-ray photoelectron spectroscopy, *J. Vac. Sci. Technol. A*, 2003, **21**, 274–283.
51. A. Jablonski and C. J. Powell, Effective attenuation lengths for quantitative determination of surface composition by Auger electron spectroscopy and X-ray photoelectron spectroscopy, *J. Electron Spectros. Relat. Phenom.*, 2017, **218**, 1–12.
52. S. Zhou, G. S. Jackson and B. Eichhorn, AuPt Alloy Nanoparticles for CO-Tolerant Hydrogen Activation: Architectural Effects in Au-Pt Bimetallic Nanocatalysts, *Adv. Func. Mater.*, 2007, **17**, 3099–3104.
53. S. Divi and A. Chatterjee, Understanding Segregation Behavior in AuPt, NiPt, and AgAu Bimetallic Nanoparticles Using Distribution Coefficients, *J. Phys, Chem. C*, 2016, **120**, 27296–27306.
54. M. T. M. Koper, Structure sensitivity and nanoscale effects in electrocatalysis, *Nanoscale*, 2011, **3**, 2054–2073.
55. A. Ferre-Vilaplana, J. V. Perales-Rondon, C. Buso-Rogero, J. M. Feliu and E. Herrero, Formic acid oxidation on platinum

electrodes: a detailed mechanism supported by experiments and calculations on well-defined surfaces, *J. Mater. Chem. A*, 2017, **5**, 21773–21784.

56. A. Capon and R. Parsons, The oxidation of formic acid at noble metal electrodes. Part III. Intermediates and mechanism on platinum electrodes, *J. Electroanal. Chem. Interfacial Electrochem.*, 1973, **45**, 205–231.
57. M. Neurock, M. Janik and A. Wieckowski, A first principles comparison of the mechanism and site requirements for the electrocatalytic oxidation of methanol and formic acid over Pt, *Faraday Discuss.*, 2009, **140**, 363–378.
58. A. Cuesta, M. Escudero, B. Lanova and H. Baltruschat, Cyclic Voltammetry, FTIRS, and DEMS Study of the Electrooxidation of Carbon Monoxide, Formic Acid, and Methanol on Cyanide-Modified Pt(111) Electrodes, *Langmuir*, 2009, **25**, 6500–6507.
59. P. N. Duchesne, Z. Y. Li, C. P. Deming, V. Fung, X. Zhao, J. Yuan, T. Regier, A. Aldalbahi, Z. Almarhoon, S. Chen, D. Jiang, N. Zheng and P. Zhang, Golden single-atomic-site platinum electrocatalysts, *Nat. Mater.*, 2018, **17**, 1033–1039.
60. A. A. Topalov, S. Cherevko, A. R. Zeradjanin, J. C. Meier, I. Katsounaros and K. J. J. Mayrhofer, Towards a comprehensive understanding of platinum dissolution in acidic media, *Chem. Sci.*, 2014, **5**, 631–638.
61. H. Li, K. Shin and G. Henkelman, Effects of ensembles,

ligand, and strain on adsorbate binding to alloy surfaces, *J. Chem. Phys.*, 2018, **149**, 174705.

Table 1. Electrochemical surface characterization parameters for HT Pt electrodeposition onto Au_{147} DENs using the indicated number of pulses. Pt coverage, θ_{Pt}, was calculated as 1-(Au_f ECSA/Au_i ECSA) and represents the fraction of the original Au surface atoms covered by Pt. ECSAs for Au before (Au_i) and after (Au_f) HT Pt electrodeposition, as well as the associated Pt ECSAs and total AuPt NP ECSAs ($ECSA_{tot}$ = Au_f ECSA + Pt ECSA) for each pulse number, are provided in Table S1. Pt:Au_i is the ratio of the Pt ECSA to the original Au ECSA. $N_{Au,surf}$ is the number of naked Au surface atoms present after HT Pt electrodeposition and was calculated as (1-θ_{Pt}) multiplied by the number of surface atoms on the Au_{147} core (92). The $\%Pt_{surf}$ is the percentage of the NP surface atoms that are Pt and was calculated as the Pt ECSA, divided by $ECSA_{tot}$, and then multiplied by 100%.

Pulses	θ_{Pt}	**Pt:Au_i**	$N_{Au,surf}$	**$\%Pt_{surf}$**
1	0.57(3)	0.62(3)	40	59(3)
3	0.83(2)	1.25(1)	16	88(1)
5	0.91(1)	1.8(2)	8	96(1)
10	0.97(1)	2.6(1)	3	99.0(4)

Table 2. FAO-related parameters as a function of the number of HT Pt electrodeposition pulses (1 to 10) for the forward-going scan of the 20th FAO CV. E_d and E_{ind} are the potentials of the peaks associated with the direct and indirect FAO pathways, respectively. All potentials are reported relative to RHE. The ratio of the current densities for the direct (j_d) and indirect (j_{ind}) FAO peaks is represented by j_d/j_{ind}. Current densities are normalized to the Pt ECSA values in Table S3.

Pulses	E_d **(V)**	E_{ind} **(V)**	j_d/j_{ind}
1	0.419(4)	0.926(4)	5.4(7)
3	0.448(1)	0.905(8)	1.6(3)
5	0.497(5)	0.893(3)	0.69(9)
10	0.515(9)	0.860(6)	0.25(4)

Figure Captions

Scheme 1. Illustration showing the pulse sequence used to deposit Pt on AuNPs.

Figure 1. TEM micrographs and the associated size-distribution histograms for HT Pt electrodeposition onto Au_{147} DENs using the indicated number of pulses. Each histogram was obtained by sizing 200 randomly selected NPs. Aberration-corrected STEM (acSTEM) micrographs of representative particles are shown in the insets of the histograms.

Figure 2. (a) CVs recorded before and after HT Pt electrodeposition onto Au_{147} DENs using the indicated number of pulses. Peaks P1, P2, and P3 correspond to AuO_x reduction, PtO_x reduction, and Pt-H adsorption/desorption (Pt-hydride) peaks, respectively. (b) Expanded view of Peaks P1, showing that the Au_{147} NP surface is nearly completely covered after 3 to 5 HT pulses. (c) Pt coverage (θ_{Pt}) as a function of pulse number. (d) the position of Peak P2 as a function of pulse number. The electrolyte was N_2-purged 0.10 M $HClO_4$ and the scan rate was 100 mV/s.

Figure 3. (a) XPS spectra in the Au 4f and Pt 4f regions for HT Pt electrodeposition onto the Au_{147} DENs using the indicated

number of pulses. (b) Au and Pt atomic compositions as a function of pulse number. The data were obtained by integrating the peaks in (a).

Figure 4. Single-particle EDS maps for HT Pt electrodeposition onto Au_{147} DENs using 10 pulses. (a) Superposition of the Pt and Au element maps. Pt and Au are shown in red and green, respectively. Individual element maps for (b) Pt and (c) Au. (d) Line profile extracted from the map in (a). The direction of the line scan along the associated map is shown in the inset and is indicated by the arrow. An additional, higher resolution line profile is provided in Figure S4. A core@shell structure is evident in both the maps and the line scans.

Figure 5. (a) FAO scans for the AuPt DENs synthesized via HT Pt electrodeposition onto Au_{147} DENs as a function of pulse number. Just the forward-going scan of the 20^{th} FAO CV is shown. Peak positions for the (b) direct (E_d) and (c) indirect (E_{ind}) FAO pathways as a function of the number of HT Pt electrodeposition pulses. (d) The ratio of the current densities associated with the direct (j_d) and indirect (j_{ind}) FAO peaks. (e) The effects of FAO cycling on the j_d/j_{ind} ratios. (f) Expanded view of (e) for just 1 to 5 HT pulses. In all cases the electrolyte was N_2-purged

0.50 M H_2SO_4 containing 0.50 M formic acid. The scan rate was 10 mV/s.

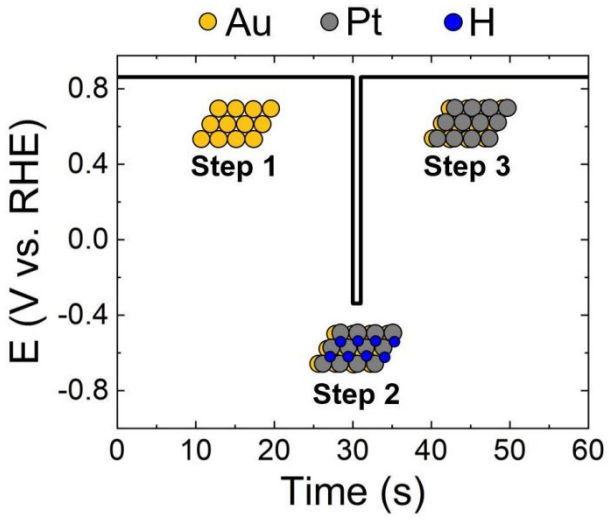
Au
Pt
H
Step 1
Step 2
Step 3
E (V vs. RHE)
0.8
0.4
0.0
-0.4
-0.8
0
10
20
30
40
50
60
Time (s)

Scheme 1.

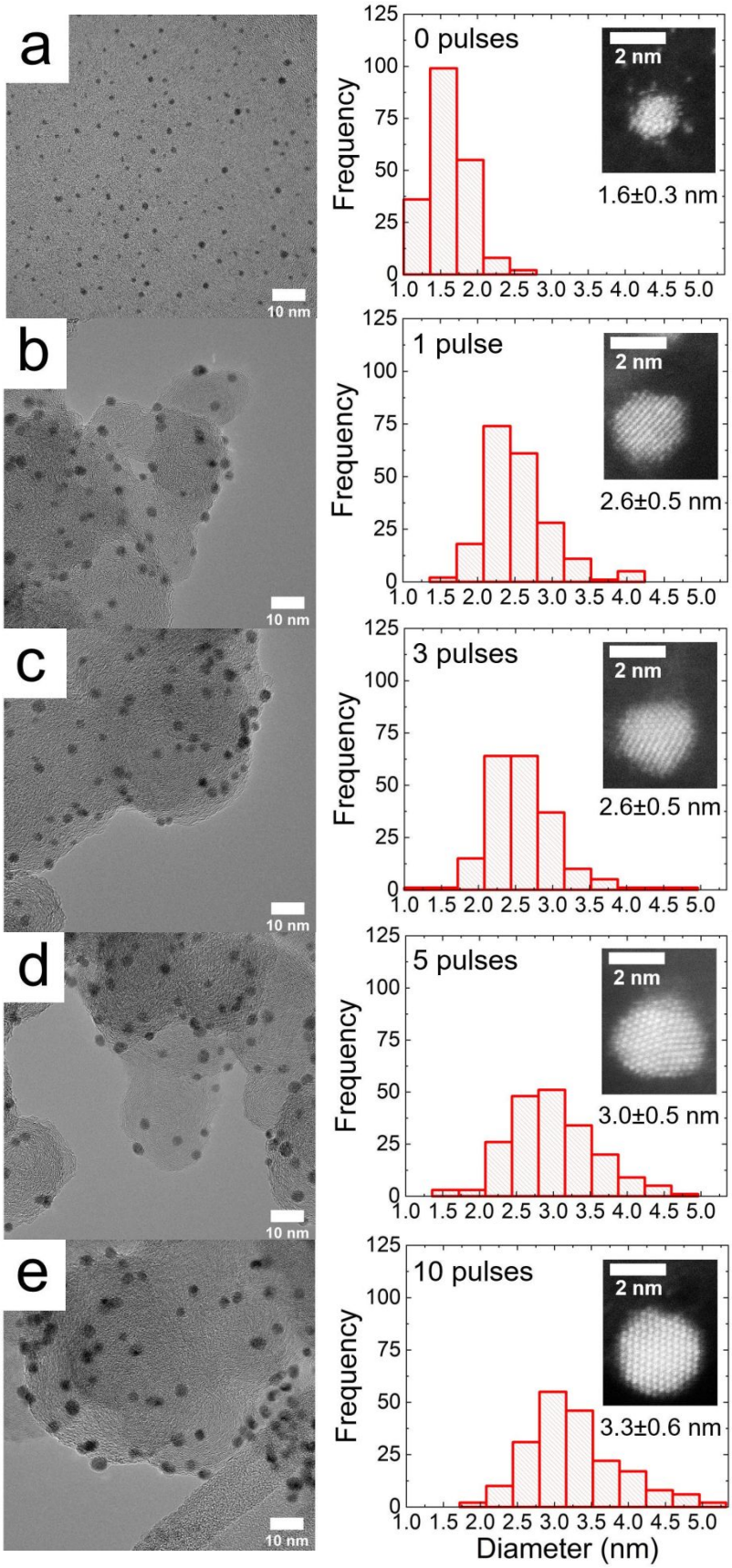
a
b
c
d
e
10 nm
0 pulses
1 pulse
3 pulses
5 pulses
10 pulses
2 nm
1.6±0.3 nm
2.6±0.5 nm
2.6±0.5 nm
3.0±0.5 nm
3.3±0.6 nm
Frequency
Diameter (nm)

Figure 1.

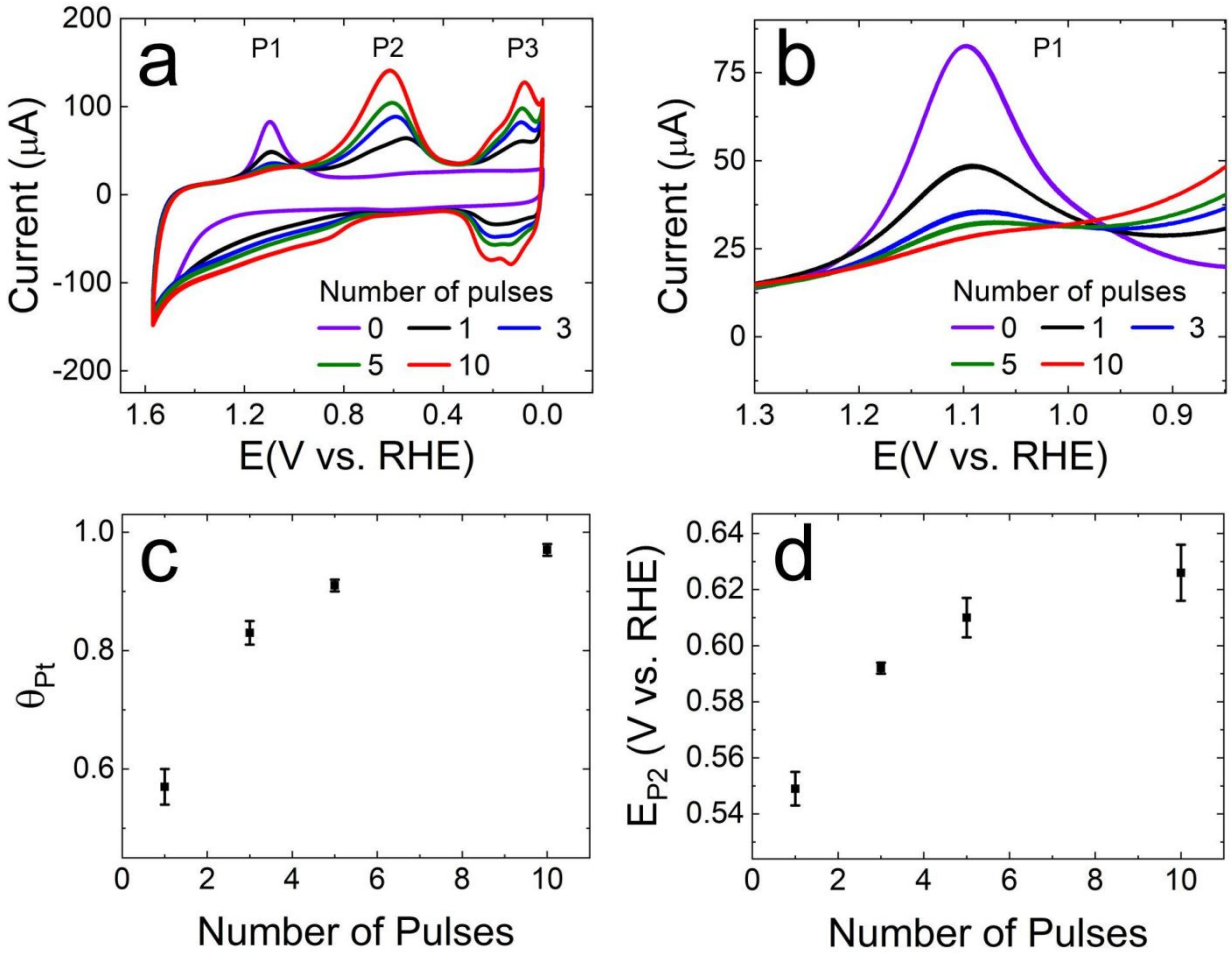
a
P1
P2
P3
Current (μA)
E(V vs. RHE)
Number of pulses
0
1
3
5
10
b
P1
Current (μA)
E(V vs. RHE)
Number of pulses
0
1
3
5
10
c
θPt
Number of Pulses
d
EP2 (V vs. RHE)
Number of Pulses

Figure 2.

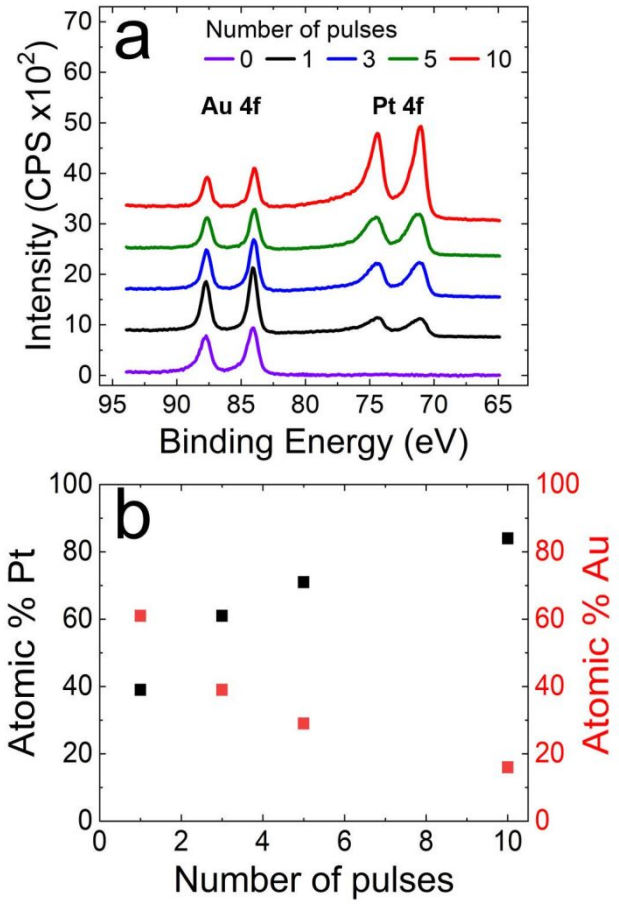
a
Number of pulses
0 1 3 5 10
Au 4f
Pt 4f
Intensity (CPS x10^2)
Binding Energy (eV)
b
Atomic % Pt
Atomic % Au
Number of pulses

Figure 3.

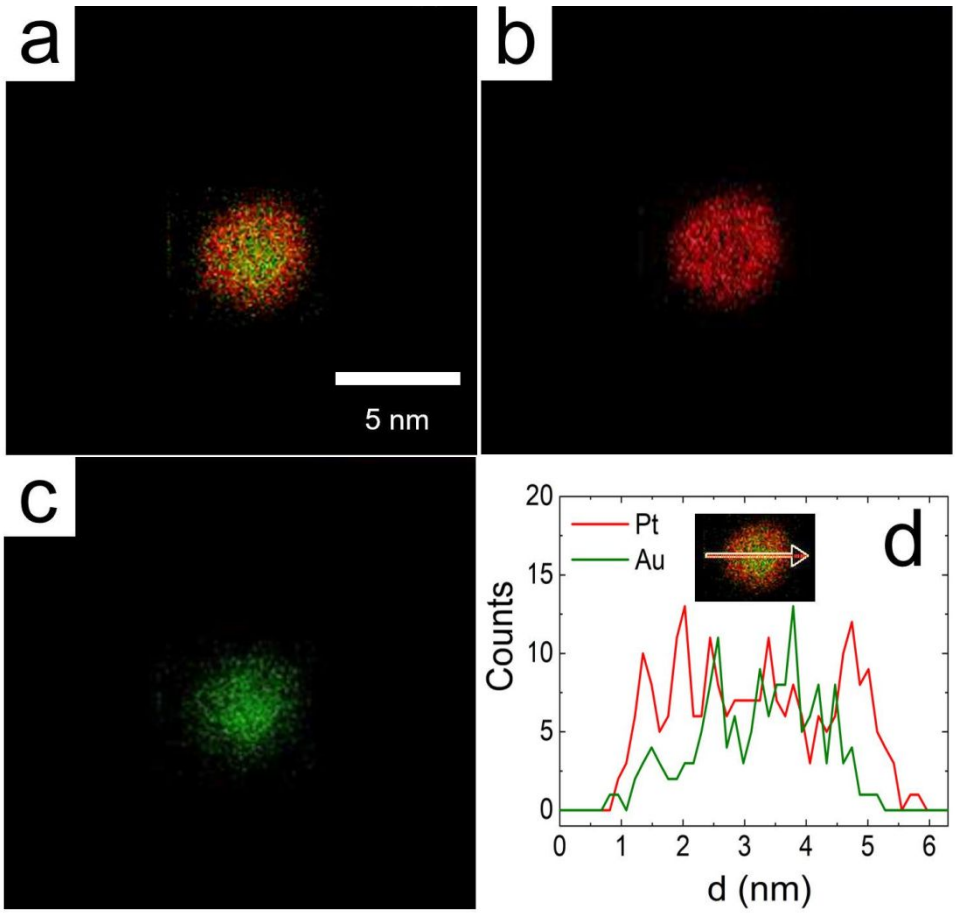

Figure 4.

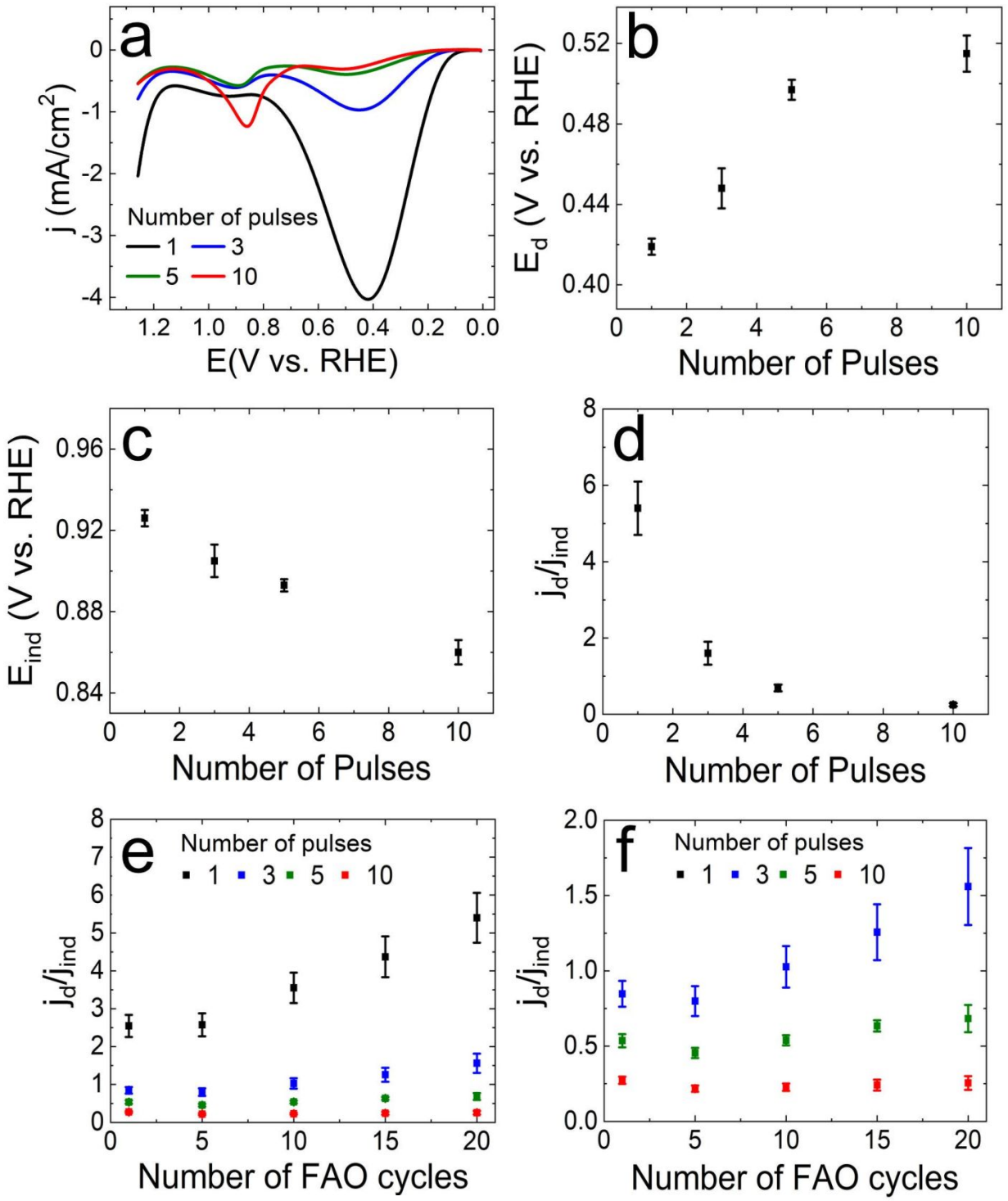
a
j (mA/cm^2)
E(V vs. RHE)
Number of pulses
1
3
5
10
b
E_d (V vs. RHE)
Number of Pulses
c
E_{ind} (V vs. RHE)
Number of Pulses
d
j_d/j_{ind}
Number of Pulses
e
j_d/j_{ind}
Number of FAO cycles
Number of pulses
1
3
5
10
f
j_d/j_{ind}
Number of FAO cycles
Number of pulses
1
3
5
10

Figure 5.

For Table of Contents only